Nanoscale

www.rsc.org/nanoscale

Volume 5 | Number 22 | 21 November 2013 | Pages 10671–11314

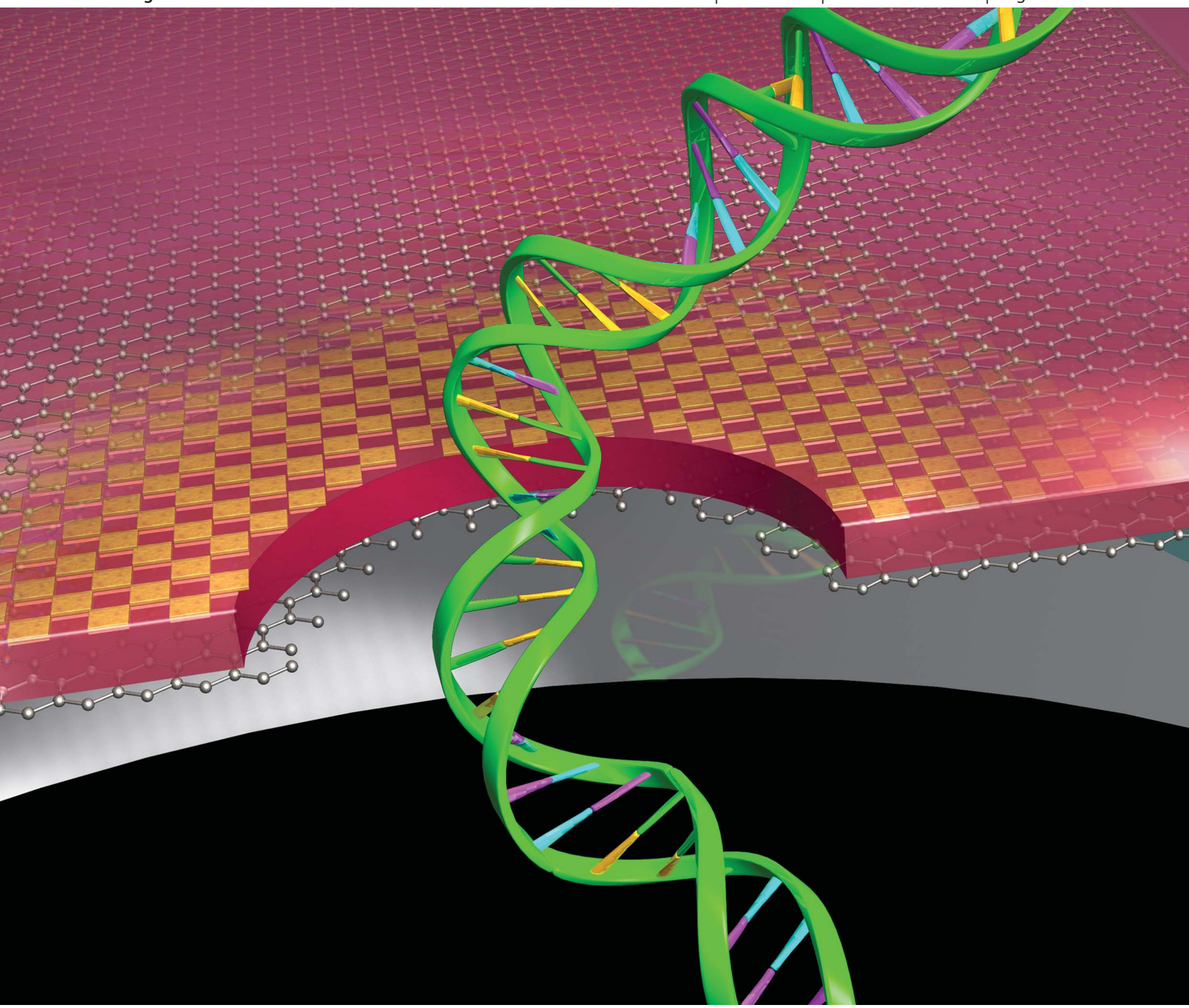

ISSN 2040-3364

RSC Publishing

PAPER

Bashir *et al.*

Electron beam induced local crystallization of HfO_2 nanopores

NCNST

2040-3364(2013)5:22;1-A

Nanoscale

RSC Publishing

PAPER

Electron beam induced local crystallization of HfO_2 nanopores for biosensing applications†

Cite this: *Nanoscale*, 2013, **5**, 10887

Jiwook Shim,‡[abc] Jose A. Rivera‡[ac] and Rashid Bashir*[abc]

We report the development of single, locally crystallized nanopores in HfO_2 membranes for biosensing applications. HfO_2 is chosen for its isoelectric point of 7.0, mechanical and chemical stability in solution, and for its potential as a high-*k* material for nanopore ionic field effect transistor applications. The HfO_2 membrane is deposited on a graphene layer suspended over a 300 nm FIB hole, where graphene is used as the mechanical support. Exposure of the membrane to a focused electron beam causes crystallization in the vicinity of the nanopore during pore formation. We investigate the effects of crystallization on the electrical and surface properties of HfO_2 films. Our surface analysis of HfO_2 reveals improved hydrophilicity of crystallized HfO_2, a notable advantage over the hydrophobicity of as-deposited HfO_2. We also demonstrate detection of dsDNA translocation through HfO_2 nanopores under various applied bias levels. In addition, our device architecture also presents a promising first step toward the realization of high-*k* HfO_2 nanopore transistors.

Received 20th May 2013
Accepted 2nd August 2013

DOI: 10.1039/c3nr02608f

www.rsc.org/nanoscale

Introduction

Nanopores continue to hold considerable promise as both a biosensing and as a DNA sequencing technology (see reviews[1–5]). The high sensitivity of solid-state nanopores has allowed for the successful detection of biomolecule complexes including RNA/antibiotic complexes,[6] RecA-coated double-stranded DNA,[7] and methylated DNA bound to methyl-CpG-binding domain proteins.[8] A recent report has also demonstrated electronic discrimination of similar genes by measuring the relative distance between γPNA probes hybridized to DNA with solid-state nanopores.[9] The interdisciplinary effort from researchers to establish solid-state nanopores as a viable sequencing platform is thriving on multiple fronts including the differentiation of short single-stranded DNA,[10] surface charge engineering for DNA capture,[11] conductance modulation[12,13] in nanopores, nanowire–nanopore transistors for localized detection,[14] and ultra-thin membrane fabrication using graphene.[15,16]

Recently, an alternative nanopore structure has evolved from the integration of graphene with solid-state membranes for both biosensing and DNA sequencing applications.[17,18] This advanced biosensing structure consists of a graphene sheet (the sensing element) embedded in between two dielectric layers which insulate the graphene from electrochemical basal plane reactions in electrolyte solution.[17] High-*k* dielectric materials are being widely adopted by the semiconductor industry for the fabrication of state-of-the-art CMOS transistors due to their superior gate oxide capacitance values when compared to traditional materials such as SiO_2. Robust, high-*k* oxides that are capable of being incorporated in aqueous environments are of interest for biosensing applications where a large gate capacitance is required. In particular, hafnium oxide (HfO_2) has attracted widespread interest by the biosensor community due to its chemical stability, pH sensitivity, and a high-*k* dielectric constant which has reported values of 20–25.[19–21] HfO_2 also has an isoelectric point of 7.0,[22] making its surface neutral at physiological pH. Thus, HfO_2 is both a suitable alternative for nanopore membrane materials and ideal for integration with stacked graphene–dielectric biosensors. While the material properties of HfO_2 are well studied and applicable in the semiconductor industry, to our knowledge, there have not been any studies done on HfO_2 as a candidate material for nanopore bio-sensing applications. In this work, we investigate the electrical properties and hydrophilicity of as-deposited and annealed HfO_2 films in solution to explore the viability of HfO_2 as both a new nanopore sensor material and a potential high-*k* nanopore transistor material. We also analyzed noise characteristics in the nanopore for annealed and as-deposited membranes to verify pore wettability. Finally, we show DNA translocation through HfO_2 nanopores.

Results and discussion

The schematic diagram in Fig. 1a shows the fabrication process for the HfO_2 membrane. A supporting 80 μm wide membrane

[a]*Department of Bioengineering, University of Illinois at Urbana-Champaign, Urbana, IL 61801, USA. E-mail: rbashir@illinois.edu*

[b]*Electrical and Computer Engineering, University of Illinois at Urbana-Champaign, Urbana, IL 61801, USA*

[c]*Micro and Nanotechnology Laboratory, University of Illinois at Urbana-Champaign, Urbana, IL 61801, USA*

† Electronic supplementary information (ESI) available. See DOI: 10.1039/c3nr02608f

‡ Authors contributed equally.

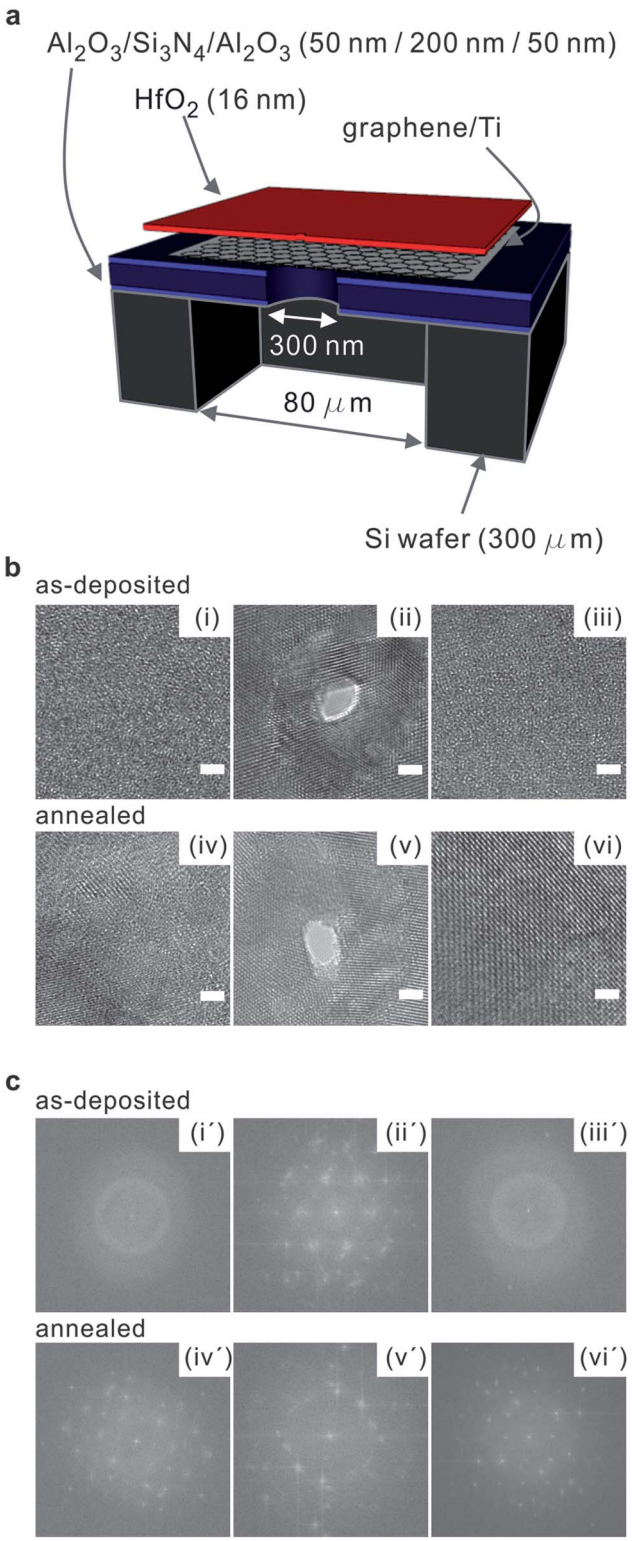

Fig. 1 Schematic of membrane fabrication and TEM images with corresponding FFT images. (a) Schematic cross-section of our membrane architecture. (b) TEM phase contrast images of as-deposited amorphous (i–iii) and annealed (iv and vi) HfO_2 films deposited on a graphene supported membrane. (i) As-deposited HfO_2 membrane before being exposed to a focused electron beam for drilling a nanopore. (ii) A nanopore drilled in amorphous HfO_2 film showing electron beam induced crystallinity in the vicinity of the pore. (iii) HfO_2 bulk phase which is ~70 nm away from a focused electron beam remains amorphous after nanopore formation. (iv) Annealed HfO_2 membrane before being exposed to a focused electron beam. (v) A nanopore was drilled in the annealed HfO_2 membrane. (vi) Annealed HfO_2 bulk phase which is ~70 nm away from a focused electron beam. (iv–vi) Annealed HfO_2 membrane showed crystallinity at all stages. (c) FFTs of corresponding TEM image found in (b) confirming amorphous (i′, iii′) and crystallized (ii′, iv′, v′, vi′) phases before and after nanopore formation.

consisting of stacked $Al_2O_3/SiN_x/Al_2O_3$ layers was suspended on a 300 μm thick Si wafer using a Bosch etching process (see Methods section for more details). The bottom Al_2O_3 layer acts as an etch stop layer for the opening of 80 μm wide backside trench by DRIE. The low stress SiN_x layer is deposited for reduced noise and increased robustness. The top Al_2O_3 layer is added as a hydrophilic layer on top of the SiN_x for improved graphene transfer process.[17] A 300 nm hole was formed in the supporting membrane using a focused ion beam. The circular shaped pore was covered by a graphene layer, on which an HfO_2 membrane was grown using atomic layer deposition.

Intrinsic stresses and pinholes present in nanolaminates are deleterious to ultra-thin membrane fabrication, a necessary step to achieving highly sensitive nanopore sensors. The high breaking and intrinsic strength of graphene[23] make the material well suited for instances where a free-standing membrane is required, as demonstrated by the recent fabrication of oxide membranes on graphene.[24] Graphene is a single layered hexagonal sheet of sp^2 hybridized carbon atoms with remarkable mechanical characteristics and electrical properties.[25] Graphene is used here for mechanical support for our HfO_2 structures but easy to drill through using the electron beam. In addition, the graphene–dielectric stack methodology leaves room for the incorporation of a gate bias in future applications where conductance modulation is required. HfO_2 was deposited using atomic layer deposition (ALD) on a graphene surface. ALD was chosen since it allows for conformal, low temperature, and sub-nanometer deposition control. The lack of dangling bonds on the basal plane of graphene makes atomic layer deposition difficult since there are no available sites for nucleation.[26] For this reason, a thin metal seed layer was evaporated on graphene. Titanium was chosen as the seed layer due to its high adsorption energy on graphene[27] and low surface diffusion.[28] The 2 nm film of titanium was oxidized once exposed to air, resulting in a thin layer of TiO_2 on the graphene surface.

The composite membrane was then imaged using transmission electron microscopy (TEM). Fig. 1b and c show TEM images and corresponding FFT images, respectively. The as-deposited HfO_2 membrane on the functionalized graphene surface is shown in Fig. 1b(i–iii). Fig. 1b(i) shows the HfO_2 membrane before drilling a nanopore, where the amorphous phase of the as-deposited membrane was observed using TEM and confirmed by taking a Fast Fourier Transform (FFT) depicted in Fig. 1b(i′). Fig. 1b(ii) and c(ii′) depict changes in membrane structure after being exposed to a focused electron beam for drilling a nanopore. Crystallization of the as-deposited film was observed in the vicinity of the nanopore in as-deposited membrane after pore formation. This was a very interesting finding because as-deposited HfO_2 films prepared by atomic layer deposition are typically amorphous and known to

crystallize in the monoclinic phase at relatively low temperatures (~500 °C).[29,30] To verify if the crystallization was formed by nanopore drilling process, another region on the same membrane, ~70 nm away from nanopore region, was examined and it remained in the as-deposited amorphous phase as shown in Fig. 1b(iii) and confirmed by 1c(iii′). As a control, nanopores were drilled in membranes annealed at 500 °C. The crystallized membranes are shown in Fig. 1b(iv–vi) and c(iv′–vi′). Annealed membranes exhibited a crystalline pattern before being exposed to the focused electron beam as shown in Fig. 1b(iv). The corresponding FFT images confirm the crystalline structure of annealed HfO_2 membranes as shown in Fig. 1c(iv′–vi′). We further investigated with SiN_x membranes (Protochips, NC), and as expected, found no crystallization in the membrane after drilling a nanopore (see ESI Fig. S1†). Previously, a study on Al_2O_3 reported hexagonal nanocrystallites in the vicinity of a nanopore in Al_2O_3 membrane, while SiN membrane found no crystallinity after pore formation.[31] However, crystallization in the vicinity of the nanopore is a unique characteristic of as-deposited HfO_2 membranes after being exposed to a focused electron beam for pore formation. We demonstrated the electron beam induced local-crystallization in the vicinity of the nanopore area in HfO_2 membranes on graphene, and it is postulated that the local-crystallization is a result of heating from the electron beam irradiation.[32,33] In the past, reports have shown that heat treatment of HfO_2 films results in improved electrical characteristics due to reduced oxygen vacancies, passivation of interface traps, and overall improvement in dielectric constant.[34] However, there is also the possibility of introducing oxygen depleted states through grain boundary formation during the heating phase.[35] Increased hydrophilicity of insulators, an essential material property for nanopore sensors due to the spontaneous evaporation of water in confined nanoscale spaces,[36] has also been attributed to high temperature annealing.

To study the effects of crystallization on the electrical properties of HfO_2, we annealed HfO_2 films deposited by atomic layer deposition in Ar/H_2 gas for 20 minutes at 500 °C and 700 °C. As-deposited and annealed HfO_2 films were characterized in an electrolyte–oxide–silicon configuration to ascertain dielectric quality under nanopore experimental conditions (typically 1 M KCl, pH 7.4). 16 nm thick HfO_2 films were deposited on polished, highly doped p-type silicon (p < 5 mohm cm) using atomic layer deposition. The electrolyte solution (1 M KCl at pH 7.4 containing 10 mM Tris and 1 mM EDTA) was dispensed onto a 2.5 mm diameter PDMS well on the HfO_2 surface and connected using Ag/AgCl electrodes while the back of the silicon substrate was connected to ground. As shown in Fig. 2a, we first applied voltages in the range between −500 mV and +500 mV across the electrolyte–dielectric interface using Axopatch 200B (Molecular Devices, CA) and acquired the data traces through Digidata 1440A (Molecular Devices, CA). The leakage current density in this voltage range is approximately 6.6 pA mm^{-2} and 13 pA mm^{-2} for both as-deposited and 500 °C annealed (crystallized) films, but the 700 °C annealed film showed 2.8 nA mm^{-2} of leakage current at 500 mV. We further investigated the leakage current as a function of voltage using a Keithley 237 controlled by LabView software. The leakage current behavior changes drastically at 3 V where an exponential increase is observed for as-deposited HfO_2 and HfO_2 annealed at both 500 °C and at 700 °C. Annealed HfO_2 films showed intolerable leakage current. The leakage density of 500 °C crystallized HfO_2 is ~10^{-9} A mm^{-2} and 700 °C crystallized HfO_2 for ~10^{-8} A mm^{-2} at 2 V, while the as-deposited film is 10^{-11} A mm^{-2}. The increase in leakage currents at a lower voltage for annealed films is attributed to microstructural changes during the growth of grain boundaries in the dielectric after post-deposition annealing. Previous studies report similar breakdown behavior for amorphous HfO_2 films on p-type silicon in aqueous environment,[37] however our results are the first extracted in a fluidic (1 M KCl at pH 7.4) environment for crystallized films. To further investigate the feasibility of integrating a gate bias with our architecture for ionic field effect regulation in the nanopore, we measured leakage current density through the HfO_2 deposited on graphene (see ESI Fig. S2†).

In addition to analyzing electrical characteristics, we studied the effects of crystallization on the wettability of HfO_2 films. Theoretical studies predict that liquids confined in between hydrophobic surfaces with contact angles approaching 90° are prone to spontaneous evaporation.[38] The hydrophobicity of

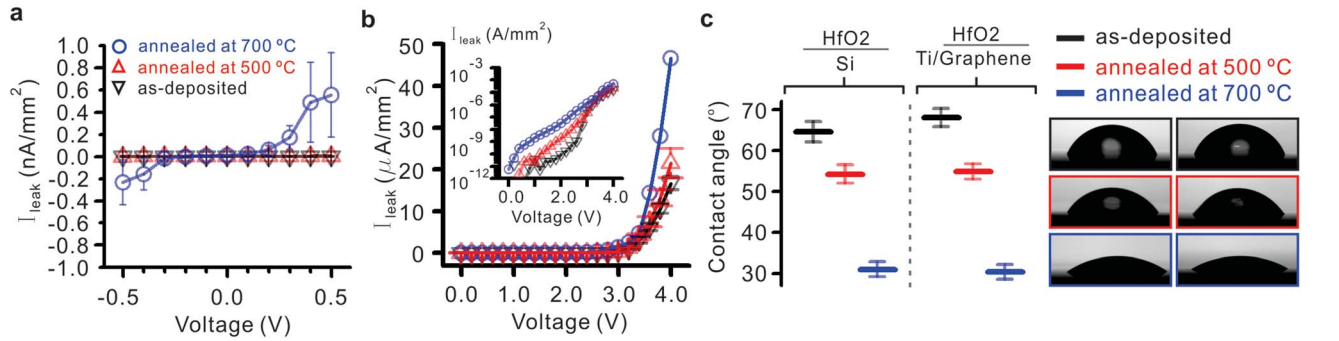

Fig. 2 Characterization of ALD HfO_2 film in an aqueous environment. (a) Leakage current densities for as-deposited and annealed HfO_2 films in an electrolyte–oxide–silicon configuration. (b) The dielectric breakdown of HfO_2 for higher voltages in 1 M KCl, where the annealed films show a higher leakage characteristic. (c) The contact angle for HfO_2 on silicon and for HfO_2 on metal-seeded graphene decreases after annealing at 500 °C and 700 °C, indicating thermo-induced hydrophilicity due to a crystal phase transition.

nanopores can be beneficial in voltage and pressure induced gating applications, however it can present a hindrance to DNA translocation nanopore experiments due to wetting difficulties. The hydrophilicity of the surface was analyzed for HfO_2 deposited on both metal-seeded graphene and p-type silicon in order to assess the impact of crystallization on nanopore functionality. The equilibrium contact angle was determined using a profile fitting method based on Young's equation. Contact angle values were measured using an Attention goniometer (Biolin Scientific, Finland). As expected, 16 nm ALD HfO_2 deposited on the graphene and silicon surfaces showed almost identical contact angle as confirmed in Fig. 2c. Interestingly, there was an increase in hydrophilicity for both surfaces after post-deposition annealing. The influence of post-deposition annealing on the contact angle of dielectric films is known as thermo-induced hydrophilicity.[39,40] This effect is attributed to the removal of surface contaminants, crystal phase transition, and changes in porosity during annealing.[39] Fig. 2c shows a contact angle difference of approximately 10° degrees for as-deposited HfO_2 in comparison with films that have been annealed at 500 °C. The contact angle for HfO_2 on p-silicon and graphene decreased to 31° and 30° respectively after annealing at 700 °C. Notably, we found that traditionally used Si_3N_4 films are much more hydrophobic with contact angles of 75° (see ESI Fig. S3†). Similar to earlier reports on thermo-induced hydrophilicity, increasing annealing temperature results in superior hydrophilicity of the oxide film. Hence, increased hydrophilicity and improved wettability is expected in the pore region due to localized heating and subsequent crystallization resulting from electron beam irradiation.[41]

In solid state nanopores, 1/*f* noise has been attributed to a variety of physical factors including surface charge fluctuations[42] as well as the mobility of charge carriers[43] at the nanopore surface. Excessive 1/*f* noise has also been attributed to nanobubbles present in the nanopore[43] and has been shown to be reduced by addition of a hydrophilic oxide layer.[44] In addition, oxygen plasma and chemical treatments are known to reduce 1/*f* noise and make the pore more hydrophilic. Fig. 3a shows a 1/*f* noise values comparison of nanopores between as-deposited and annealed HfO_2 membrane at 500 °C from 100 to 300 mV. Nanopores of similar sizes (2 × 3 nm and 2.2 × 2.8 nm pores in as-deposited and annealed HfO_2 membranes, respectively) were used for 1/*f* noise measurements. Interestingly, nanopores in both of as-deposited and annealed HfO_2 produced very similar 1/*f* noise values. Similar 1/*f* noise between as-deposited and annealed membranes confirm that the 1/*f* noise is dominated by local charge interactions in the nanopore region as opposed to being affected by the bulk phase transition. This was confirmed by imaging the local-crystallization at the nanopore region on amorphous as-deposited and crystallized HfO_2 membranes (Fig. 1b and c). In addition, Fig. 3b shows current *versus* voltage measurements for five different HfO_2 nanopore diameters. These measurements were taken by mounting the nanopore chip in between two reservoirs that were later filled with conductive electrolyte (1 M KCl at pH 7.4). Fig. 3b shows that the relationship between current and voltage for a nanopore submerged in conductive solution approximates

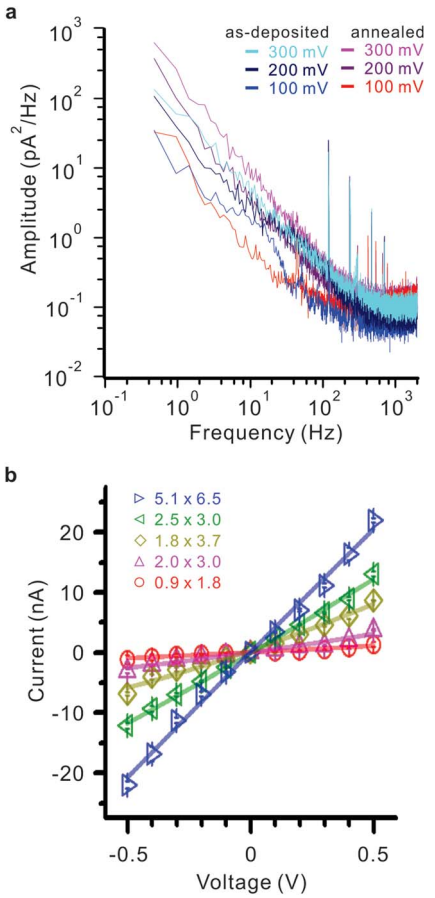

Fig. 3 Noise and *I–V* characteristics for nanopores drilled in HfO_2. (a) The magnitude of the 1/*f* noise scales with the applied voltage, indicating wettability of the pore. In comparison between annealed values and as-deposited values of 1/*f* noise are similar in magnitude, suggesting that the 1/*f* noise is dominated by ionic interactions at the crystallized nanopore as opposed to being influenced by the phase of the bulk membrane region. The nanopores used for 1/*f* noise measurement are in similar dimension. As-deposited membrane has 2 × 3 nm pore and annealed membrane has 2.2 × 2.8 nm. (b) *I–V* curve measurement for five nanopores of different sizes in 1 M KCl solution.

Ohm's law. The *I–V* measurements through multiple nanopores were in good agreement with previous findings for open pore current[45] without any asymmetric or rectifying currents.

Furthermore, we detected dsDNA translocation with our HfO_2 nanopore sensor. The experiment was performed in 1 M KCl, 10 mM Tris, 1 mM EDTA, pH 7.4 and the concentration of DNA was 1 nM. In this experiment, 1 kbp dsDNA was introduced to the *cis* side of the chamber followed by an applied bias of 500 mV at the *trans* side. Applying negative voltages to the *trans* side or replacing the dsDNA with blank 1 M KCl solution resulted in no current blockages, indicating that the observed events are from DNA translocation. The magnitude of the translocation event will depend on the pore geometry and size of the translocating molecule.

Assuming a cylindrical geometry, the ionic current through a circular nanopore is defined by $= \frac{\sigma A V}{l}$, where σ is the conductivity of the electrolyte solution, A is the cross-sectional area of the nanopore, V is the applied bias, and l is the length of

the pore. Consequently, the percent change in open pore current follows the relationship $\frac{\Delta I}{I} = \frac{\Delta A}{A}$ where ΔA and A are the cross-sectional area of the molecule and nanopore, respectively.[46] Hundreds of events were detected with numbers in proportion to the applied voltage level; 172 events at 200 mV, 92 at 300 mV, 118 at 400 mV and 351 at 500 mV. Fig. 4a shows representative ionic current traces of 1 kbp dsDNA through a 4 nm pore in HfO_2 membrane. The nanopore ionic signature shows decrease in magnitude with decreasing voltage, indicating that DNA molecules are directly changing the ionic conductance of the nanopore. Fig. 4b shows a set of current blockade values resulting from applied voltages in the range of 200–500 mV. Current blockades were obtained fitting a Gaussian function to peak blocking current, and showed nanopore ionic current blocking of 285.5 pA at 200 mV, 384.9 pA at 300 mV, 515.3 pA at 400 mV and 623.8 pA at 500 mV, which are in good agreement with the standard geometric model (see ESI Fig. S4†). In addition, there is a translocation dwell time associated with each applied voltage. Ionic current signature shows shortened translocation duration with increasing voltage, indicating that translocations of DNA molecules are voltage-driven. Fig. 4c shows a set of translocation duration values obtained by exponential fittings to translocation dwell time in applied voltages from 200 mV to 500 mV. The obtained duration values were 318 μs at 200 mV, 115 μs at 300 mV, 88 μs at 400 mV and 58 μs at 500 mV (see ESI Fig. S4†). The trend of decrease in translocation duration with increasing voltage can be well fitted to an exponential function, which is found in previous report and expected in translocation of DNA through solid-state nanopores.[47]

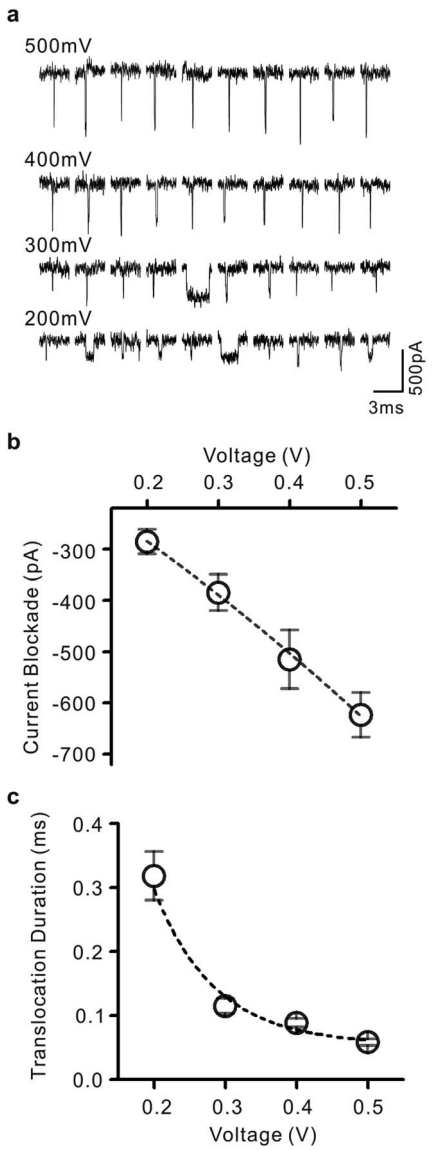

Fig. 4 Double-stranded DNA translocation. (a) Representative data traces showing translocation of 1 kbp dsDNA through a 4 nm pore in HfO_2 membrane. Nanopore ionic currents were recorded in 1 M KCl at pH 7.4 containing 10 mM Tris and 1 mM EDTA at voltages in range from 200 mV to 500 mV. (b) Current blockade levels for DNA translocation events plotted as a function of voltage. (c) Translocation durations of the events corresponding to four different voltages. The values of current blockades and translocation durations were obtained by fitting to a Gaussian function and an exponential function, respectively.

Conclusions

The aim of this work was to demonstrate DNA detection using HfO_2 based nanopore sensors. Graphene, a single layered hexagonal sheet of sp^2 carbon atoms grown by chemical vapor deposition, was used as a structural support in the fabrication of HfO_2 membranes. Transmission electron microscopy was used to drill a single nanometer sized hole in the membrane. Locally induced crystallization of HfO_2 was observed upon prolonged exposure of the electron beam during nanopore drilling, a consequence that is attributed to localized heating. In order to elucidate the effects of crystallization on the electrical and surface properties of HfO_2, ultra-thin films were deposited *via* atomic layer deposition on p-type silicon and characterized in 1 M KCl solution. Leakage currents were analyzed for annealed and as-deposited films, revealing higher current densities in crystallized films due to the nucleation of grain boundaries.

However, crystallization of the high k dielectric resulted in increased hydrophilicity, suggesting improved wettability in HfO_2 nanopores. Power spectral density plots were acquired and the $1/f$ noise was shown to scale under increasing applied voltages for both as-deposited and annealed films, suggesting good pore wettability. Finally, the viability of HfO_2 nanopores as a biosensing platform was verified by performing DNA translocation experiments. We conclude that HfO_2 is a suitable material for nanopore sensing applications due to its potential in high-k nanopore transistor applications, thermo-induced hydrophilicity, chemical inertness, and the ability to detect DNA transport.

Methods

Supporting membrane fabrication

Supporting membrane fabrication process has been introduced in previous study,[17] and brief description is as follow. Membranes were fabricated on 300 ± 2 μm thick double-side polished ⟨100⟩ silicon wafers (Quest International). Wafers were

cleaned in piranha solution (1 : 2 ratios of H_2SO_4 and H_2O_2) for 15 minutes, DI-water rinsed and air-gun dried before depositing Al_2O_3 *via* Atomic Layer Deposition (ALD Cambridge Nanotech). 50 nm of Al_2O_3 was deposited at a platen temperature of 250 °C using tetramethylaluminum (TMA) and water vapor precursors. Subsequently, 200 nm of low-stress SiN_x was deposited (STS Mesc PECVD system) using a mixed-frequency recipe (high frequency, 6 s at 13.56 MHz, platen power of 20 W; and low frequency, 2 s at 380 kHz, platen power of 60 W) with precursors silane (SiH_4) and ammonia (NH_3) at flow rates of 40 and 55 sccm, respectively, at a platen temperature of 300 °C. Another 50 nm of Al_2O_3 is deposited *via* ALD on the SiN_x layer as described above, resulting in stacked $Al_2O_3/SiN_x/Al_2O_3$ layers. The backside of the wafer is then spin-coated with Megaposit SPR220 photoresist (3000 rpm at 30 s followed by soft bake at 60 °C for 2 min and 110 °C for 1 min). Optical lithography is used to pattern 80 μm square windows on the backside of the water while the front side is protected with KMPR 1000 photoresist. The wafer is later placed into an STS Pegasus ICP DRIE and back-etched for 22 minutes using a Bosch etching process. This process results in the suspension of 80 μm wide square membrane of stacked layers (the bottom Al_2O_3 layer serves as a stop layer). Finally, a focused ion beam (FEI FIB DB235) operated at a beam current of 30 pA is used to form 300 nm hole on the suspended stacked membrane.

Graphene and HfO_2 nanopore fabrication

Graphene was grown *via* chemical vapor deposition (CVD) on 1.4 mil copper foil (Alfa Aesar). The copper foil was placed in an Atomate CVD furnace and annealed at 1000 °C under Ar/H_2 flow for 90 minutes at a base pressure of ~4.4 Torr in order to increase the copper grain size. Graphene is grown for 50 minutes at 1000 °C under 125 sccm of CH_4 and 50 sccm of H_2 at a base pressure of about 2.5 Torr. Once the graphene is grown on the copper, the substrate is cooled to room temperature under 500 sccm of Ar while the base pressure is ramped up to 760 Torr. The copper foil is then coated with two layers of PMMA (295 K A2 and 950 K A4). Both layers are spun at 3000 rpm for 30 seconds and soft-baked for 2 minutes at 200 °C. The graphene grown on the backside of the copper foil is then etched away by an O_2 plasma etching process (Plasmatherm Freon RIE). After graphene removal from the backside, the copper is etched away overnight in $FeCl_3$ solution (Transcene CE-100). The resulting graphene film protected by the PMMA bilayer is then transferred from the copper etchant to DI water using a piranha-cleaned (1 : 2 ratio of H_2SO_4 : H_2O_2) glass slide.

Subsequently, the film is transferred to 10% hydrochloride (HCl) solution diluted in DI water to remove residual metal particles followed by a second DI water rinse. The film is then transferred onto a 12 × 12 mm chip with our predefined FIB holes (about 300 nm in diameter) and the PMMA is removed by submerging the chip in 1 : 1 methylene chloride–methanol solution for 30 minutes. The samples are subsequently annealed in an Ar (500 sccm)/H_2 (100 sccm) environment for 1.5 hours to remove PMMA residue from the surface. Samples were then placed inside of a CHA SEC-600 electron beam evaporator after the graphene transfer and anneal was completed. An ultra-thin, 2 nm seed layer of titanium oxide (TiO_2) was evaporated over the graphene substrate at a rate of 0.2 A s^{-1}. The graphene/TiO_2 chips were then placed inside an ALD reactor and 16 nm of HfO_2 was deposited over the surface at a platen temperature of 200 °C. Single nanopores ranging from 1 to 5 nm in diameter were drilled using a transmission electron microscope (JEOL 2010F field-emission gun) operated at 200 kV in convergent beam electron diffraction (CBED) mode with a focused electron probe of diameter ~1.5 nm. An O_2 plasma treatment on the backside of the chip was performed at 50 W for 30 s to remove hydrophobic graphene layer and to facilitate nanopore wetting.

Acknowledgements

The authors would like to acknowledge funding support from Oxford Nanopore Technologies, U.K and the National Institutes of Health (Grant # R21 CA155863). The authors would also like to acknowledge valuable discussions with Shouvik Banerjee and David Estrada. In addition, the support from the staff of the Micro and Nanotechnology Laboratory (MNTL) is greatly appreciated.

References

1 B. M. Venkatesan and R. Bashir, Nanopore sensors for nucleic acid analysis, *Nat. Nanotechnol.*, 2011, **6**, 615–624.
2 D. Branton, *et al.*, The potential and challenges of nanopore sequencing, *Nat. Biotechnol.*, 2008, **26**, 1146–1153.
3 M. Wanunu, Nanopores: A journey towards DNA sequencing, *Phys. Life Rev.*, 2012, **9**, 125–158.
4 L. Q. Gu and J. W. Shim, Single molecule sensing by nanopores and nanopore devices, *Analyst*, 2010, **135**, 441–451.
5 S. Howorka and Z. Siwy, Nanopore analytics: sensing of single molecules, *Chem. Soc. Rev.*, 2009, **38**, 2360–2384.
6 M. Wanunu, *et al.*, Nanopore Analysis of Individual RNA/Antibiotic Complexes, *ACS Nano*, 2011, **5**, 9345–9353.
7 R. M. M. Smeets, S. W. Kowalczyk, A. R. Hall, N. H. Dekker and C. Dekker, Translocation of RecA-Coated Double-Stranded DNA through Solid-State Nanopores, *Nano Lett.*, 2009, **9**, 3089–3095.
8 J. Shim, *et al.*, Detection and Quantification of Methylation in DNA using Solid-State Nanopores, *Sci. Rep.*, 2013, **3**, 1389.
9 A. Singer, S. Rapireddy, D. H. Ly and A. Meller, Electronic Barcoding of a Viral Gene at the Single-Molecule Level, *Nano Lett.*, 2012, **12**, 1722–1728.
10 K. Venta, *et al.*, Differentiation of Short, Single-Stranded DNA Homopolymers in Solid-State Nanopores, *ACS Nano*, 2013, **7**, 4629–4636.
11 K. H. Paik, *et al.*, Control of DNA Capture by Nanofluidic Transistors, *ACS Nano*, 2012, **6**, 6767–6775.
12 Z. J. Jiang and D. Stein, Charge regulation in nanopore ionic field-effect transistors, *Phys. Rev. E: Stat., Nonlinear, Soft Matter Phys.*, 2011, **83**, 031203.
13 S. W. Nam, M. J. Rooks, K. B. Kim and S. M. Rossnagel, Ionic Field Effect Transistors with Sub-10 nm Multiple Nanopores, *Nano Lett.*, 2009, **9**, 2044–2048.

14 P. Xie, Q. H. Xiong, Y. Fang, Q. Qing and C. M. Lieber, Local electrical potential detection of DNA by nanowire–nanopore sensors, *Nat. Nanotechnol.*, 2012, **7**, 119–125.

15 G. F. Schneider, *et al.*, DNA Translocation through Graphene Nanopores, *Nano Lett.*, 2010, **10**, 3163–3167.

16 C. A. Merchant, *et al.*, DNA Translocation through Graphene Nanopores, *Nano Lett.*, 2010, **10**, 2915–2921.

17 S. Banerjee, *et al.*, Electrochemistry at the Edge of a Single Graphene Layer in a Nanopore, *ACS Nano*, 2013, **7**, 834–843.

18 B. M. Venkatesan, *et al.*, Stacked Graphene-Al_2O_3 Nanopore Sensors for Sensitive Detection of DNA and DNA–Protein Complexes, *ACS Nano*, 2012, **6**, 441–450.

19 B. R. Dorvel, *et al.*, Silicon Nanowires with High-k Hafnium Oxide Dielectrics for Sensitive Detection of Small Nucleic Acid Oligomers, *ACS Nano*, 2012, **6**, 6150–6164.

20 G. D. Wilk, R. M. Wallace and J. M. Anthony, High-kappa gate dielectrics: Current status and materials properties considerations, *J. Appl. Phys.*, 2001, **89**, 5243–5275.

21 J. Robertson, High dielectric constant oxides, *Eur. Phys. J.: Appl. Phys.*, 2004, **28**, 265–291.

22 G. A. Parks, The Isoelectric Points of Solid Oxides Solid Hydroxides and Aqueous Hydroxo Complex Systems, *Chem. Rev.*, 1965, **65**, 177–198.

23 C. Lee, X. D. Wei, J. W. Kysar and J. Hone, Measurement of the elastic properties and intrinsic strength of monolayer graphene, *Science*, 2008, **321**, 385–388.

24 L. D. Wang, *et al.*, Ultrathin Oxide Films by Atomic Layer Deposition on Graphene, *Nano Lett.*, 2012, **12**, 3706–3710.

25 Y. B. Zhang, Y. W. Tan, H. L. Stormer and P. Kim, Experimental observation of the quantum Hall effect and Berry's phase in graphene, *Nature*, 2005, **438**, 201–204.

26 B. Fallahazad, *et al.*, Scaling of Al_2O_3 dielectric for graphene field-effect transistors, *Appl. Phys. Lett.*, 2012, **100**, 093112.

27 K. T. Chan, J. B. Neaton and M. L. Cohen, First-principles study of metal adatom adsorption on graphene, *Phys. Rev. B: Condens. Matter Mater. Phys.*, 2008, **77**, 235430.

28 A. Matsubayashi, J. Abel, D. P. Sinha, J. U. Lee and V. P. LaBella, Characterization of metal oxide layers grown on CVD graphene, *J. Vac. Sci. Technol., A*, 2013, **31**, 021506.

29 H. Kim, P. C. McIntyre and K. C. Saraswat, Effects of crystallization on the electrical properties of ultrathin HfO_2 dielectrics grown by atomic layer deposition, *Appl. Phys. Lett.*, 2003, **82**, 106–108.

30 H. Kim, A. Marshall, P. C. McIntyre and K. C. Saraswat, Crystallization kinetics and microstructure-dependent leakage current behavior of ultrathin HfO_2 dielectrics: In situ annealing studies, *Appl. Phys. Lett.*, 2004, **84**, 2064–2066.

31 B. M. Venkatesan, *et al.*, Highly Sensitive, Mechanically Stable Nanopore Sensors for DNA Analysis, *Adv. Mater.*, 2009, **21**, 2771–2776.

32 L. C. Liu and S. H. Risbud, Real-Time Hot-Stage High-Voltage Transmission Electron-Microscopy Precipitation of CdS Nanocrystals in Glasses – Experiment and Theoretical-Analysis, *J. Appl. Phys.*, 1994, **76**, 4576–4580.

33 T. Yokota, M. Murayama and J. M. Howe, In situ transmission-electron-microscopy investigation of melting in submicron Al-Si alloy particles under electron-beam irradiation, *Phys. Rev. Lett.*, 2003, **91**, 265504.

34 W. L. Yang, J. Marino, A. Monson and C. A. Wolden, An investigation of annealing on the dielectric performance of TiO_2 thin films, *Semicond. Sci. Technol.*, 2006, **21**, 1573–1579.

35 H. S. Baik, *et al.*, Interface structure and non-stoichiometry in HfO_2 dielectrics, *Appl. Phys. Lett.*, 2004, **85**, 672–674.

36 S. Smirnov, I. Vlassiouk, P. Takmakov and F. Rios, Water Confinement in Hydrophobic Nanopores. Pressure-Induced Wetting and Drying, *ACS Nano*, 2010, **4**, 5069–5075.

37 F. Wallrapp and P. Fromherz, TiO_2 and HfO_2 in electrolyte-oxide-silicon configuration for applications in bioelectronics, *J. Appl. Phys.*, 2006, **99**, 114103.

38 A. Luzar, Activation barrier scaling for the spontaneous evaporation of confined water, *J. Phys. Chem. B*, 2004, **108**, 19859–19866.

39 Q. Ye, P. Y. Liu, Z. F. Tang and L. Zhai, Hydrophilic properties of nano-TiO_2 thin films deposited by RF magnetron sputtering, *Vacuum*, 2007, **81**, 627–631.

40 R. Azimirad, N. Naseri, O. Akhavan and A. Z. Moshfegh, Hydrophilicity variation of WO_3 thin films with annealing temperature, *J. Phys. D: Appl. Phys.*, 2007, **40**, 1134–1137.

41 H. M. Kim, M. H. Lee and K. B. Kim, Theoretical and experimental study of nanopore drilling by a focused electron beam in transmission electron microscopy, *Nanotechnology*, 2011, **22**, 275303.

42 D. Stein, M. Kruithof and C. Dekker, Surface-charge-governed ion transport in nanofluidic channels, *Phys. Rev. Lett.*, 2004, **93**, 035901.

43 R. M. M. Smeets, U. F. Keyser, M. Y. Wu, N. H. Dekker and C. Dekker, Nanobubbles in solid-state nanopores, *Phys. Rev. Lett.*, 2006, **97**, 088101.

44 P. Chen, *et al.*, Atomic layer deposition to fine-tune the surface properties and diameters of fabricated nanopores, *Nano Lett.*, 2004, **4**, 1333–1337.

45 R. M. M. Smeets, *et al.*, Salt dependence of ion transport and DNA translocation through solid-state nanopores, *Nano Lett.*, 2006, **6**, 89–95.

46 A. J. Storm, J. H. Chen, H. W. Zandbergen and C. Dekker, Translocation of double-strand DNA through a silicon oxide nanopore, *Phys. Rev. E: Stat., Nonlinear, Soft Matter Phys.*, 2005, **71**, 051903.

47 M. Wanunu, J. Sutin, B. McNally, A. Chow and A. Meller, DNA Translocation Governed by Interactions with Solid-State Nanopores, *Biophys. J.*, 2008, **95**, 4716–4725.